Influence of Ta substitution for Nb in $Zn_3Nb_2O_8$ and the impact on the crystal structure and

microwave dielectric properties

Yonggui Zhao, Ping Zhang*

School of Electronic and Information Engineering and Key Laboratory of Advanced Ceramics and

Machining Technology of Ministry of Education, Tianjin University, Tianjin 300072, P. R. China

Abstract

Dependence of microwave dielectric properties on the structural characteristics of

$Zn_3(Nb_{1-x}Ta_x)_2O_8$ (x=0.02-0.10) ceramics were prepared via a solid-state reaction route. From XRD

patterns, single $Zn_3Nb_2O_8$ phase with layered crystal structures was formed in ceramic samples with

0.02≤x≤0.10. The Raman spectrum was firstly used to analyze the vibrational phonon modes of the

$Zn_3Nb_2O_8$ samples. Based on the P-V-L dielectric theory, the intrinsic factors influenced the microwave

dielectric properties were systematically investigated. According to the calculated results, the

experiment dielectric constant had a closely relationship with the theoretical dielectric constant. The

Nb-site lattice energy was found to be as a vital factor to explain the change of the Q×f value. With the

Nb-site bond energy increased, the |τ_f| value decreased which indicates that higher bond energy would

correlate more stable system. This work presents a novel method to investigate the intrinsic factors of

the microwave dielectric properties.

Key words: Raman spectra; Chemical bond theory; Rietveld refinements; Ceramics;

1. Introduction

With the increasing of the wireless communication technology, the demand for new microwave

1

―――――――――――――――

*Corresponding author. Tel. : +86 13702194791

Email address: zptai@163.com (P. Zhang)

dielectric materials has continued. The search for novel microwave dielectric systems with ultra low dielectric loss (high quality factor Q_f) has always been a hot topic [1-4]. Niobium based oxides are well known for their importance to the electronic industry, namely in the track of new approaches for passive devices such as capacitors, radar and global positioning systems (GPS) [5-7].

The $Zn_3Nb_2O_8$ compound, which was an typical material in the niobium based oxides and shown the excellent microwave dielectric properties with ε_r = 21.6, $Q \times f$ = 83,300 GHz and τ_f = -71 ppm/°C, firstly reported by *Kim et al* [8]. In order to meet the system stability, the TiO_2 additive was used to improve the microwave dielectric properties, and the $0.275Zn_3Nb_2O_8$-$0.725TiO_2$ compounds showed a near zero τ_f value of 4 ppm/°C [9]. Latter, *Lee et al*. [10] reported that V_2O_5-doped $Zn_3Nb_2O_8$ exhibited the microwave dielectric properties of ε_r = 22.4 and $Q \times f$ = 67,500 GHz sintered at 850 °C-1000 °C. *Wu et al*. [11] lowered the sintering temperature of $Zn_3Nb_2O_8$ down to 950 °C by using 3 wt% of $0.29BaCO_3$-$0.71CuO$ additives and the lowered $Zn_3Nb_2O_8$ ceramics exhibits ε_r=14.7 and $Q \times f$= 8,200 GHz. Simple synthesis process for the $Zn_3Nb_2O_8$ ceramics was firstly reported by *Liou et al*. [12] and A maximum density 5.72 g/cm^3 (99.7% of the theoretical density) was found for pellets sintered at 1170°C for 2 h. Recently, *Huang et al*. [13-14] reported the same family of materials $(Zn_{1-x}A_x)_3Nb_2O_8$ (A= Mg^{2+}, Ni^{2+}), and discovered that the microwave dielectric properties of $Zn_3Nb_2O_8$ ceramics could be optimized using bivalent ions substituted to Zn^{2+} ionic owing to formation of solid solutions and maximum quality factor for the $Zn_3Nb_2O_8$ ceramics could be obtained with 0.05 mol Mg^{2+} additives. The effects of other bivalent ions (Co^{2+}, Mn^{2+}) on the microwave dielectric properties of $Zn_3Nb_2O_8$ ceramics were also investigated by *Li et al* [15]. However, the correlations among crystal structure, intrinsic factors and microwave dielectric properties of $Zn_3Nb_2O_8$ ceramics are not investigated in the above reports. The complex chemical bond theory was first reported by *Zhang et al* [16-19], which

2

successfully dealt with many complex multiband crystals. In our recent works, we built an close

relationship between the complex chemical bond theory and microwave dielectric ceramics, and

succeeded in solving many ceramics system, like $(Nd_{1-x}A_x)SbO_4$ (A=La^{3+}, Y^{3+}, Sm^{3+}), $Nd(Nb_{1-x}Sb_x)O_4$,

$ZnZr(Nb, Ta, Sb)_2O_8$ and $Li_2Mg(Ti_{1-x}Mn_x)_3O_8$ ceramics [20-25]. To the best of our knowledge, the

relationship between Raman spectra, complex chemical bond theory, crystal structure and the

microwave dielectric properties of $Zn_3(Nb_{1-x}Ta_x)_2O_8$ ceramics was not reported. Particularly, the

Raman scattering is not used to analyze the $Zn_3Nb_2O_8$ ceramic materials because of the intrinsic

difficulties to discern and assign the active modes of unoriented samples, in contrast to oriented

single-crystals [26].

Therefore, in view of the increasing importance of low loss $Zn_3Nb_2O_8$ ceramics for the materials

chemistry and the lacking systematic comprehensive, we prepared the $Zn_3(Nb_{1-x}Ta_x)_2O_8$ ceramics

through the conventional solid-stated route and investigated systematically the phonon modes of

$Zn_3(Nb_{1-x}Ta_x)_2O_8$ ceramics through Raman spectroscopy employed for the first time. And the

theoretical dielectric constant, lattice energy and bond energy were calculated to help us to evaluate the

intrinsic factor of microwave dielectric properties. In addition, an available method based on the

Rietveld refinement of X-ray techniques was also used to analyze the crystal structure.

2. Experimental and theory procedure

2.1 Experimental section

High-pure (>99.9%) oxide powders of ZnO, Nb_2O_5 and Ta_2O_5 were used as raw materials to

prepare the specimens. The raw materials were mixed according to the formula of $Zn_3(Nb_{1-x}Ta_x)_2O_8$

(x=0.02-0.10). Stoichiometric mixtures of starting materials were ball-milled with distilled water for 6 h.

All the slurries were dried, crushed and sieved with a 40 mesh screen. Then the sieved specimen

calcined at 1050 °C for 4 h, the obtained powders were re-milled 6 h. After drying, the crushed powders

sieved with a 40 mesh screen firstly, then with 6 wt% paraffin as a binder were granulated by sieved

with an 80 mesh screen. The powders after sieved were pressed into disk-typepellets with 10 mm

diameter and 5 mm thickness at 100 MPa. Then these pellets were sintered at temperatures of 1175°C

for 4 h in air with the heating rate of 5 $^{\circ}$C/min.

The crystalline phases of the sintered samples were identified by X-ray diffraction (XRD, Rigaku

D/max 2550 PC, Tokyo, Japan) with Cu Kα radiation generated at 200 kV and 100 mA. Diffraction

patterns were obtained between 10 and 60° (2θ) using a step-scan method with 0.02°/3s. The

microstructure of the ceramic surfaces were performed and analyzed by a scanning electron microscopy

(SEM, MERLIN Compact, Germany). A Horiba Jobin Yvon HR800 UV Raman spectrometer equipped

with a Peltier-cooled charge-coupled device detector was used to collect Raman spectra of polished and

thermally etched $Zn_3(Nb_{1-x}Ta_x)_2O_8$ (x=0.02-0.10) compositions. The microwave dielectric properties

were measured in the frequency range of 8-13 GHz using a HP8720ES network analyzer. The

temperature coefficients of resonant frequency (τ_f) were measured in the temperature range from 25 °C

to 85 °C. The τ_f (ppm/ °C) was calculated by noting the change in resonant frequency (Δf)

$$\tau_f = \frac{f_2 - f_1}{f_1(T_2 - T_1)} \tag{1}$$

where f_1 is resonant frequency at 85°C and f_2 is the resonant frequency at 25°C respectively.

The bulk densities of the sintered samples were measured using the Archimedes method. To study

the relative density of the sample, the theoretical density was obtained from the following:

$$\rho_{theory} = \frac{ZA}{V_C N_A} \tag{2}$$

where V_C, N_A, Z, and A are volume of unit cell (cm^3), avogadro number (mol^{-1}), number of atoms in unit

4

cell, and atomic weight (g/mol), respectively.

The relative density was calculated by the Eq. (3):

$$\rho_{relative} = \frac{\rho_{bulk}}{\rho_{theory}} \times 100\% \qquad\qquad (3)$$

2.2 Theory development

In our previous work, we have successfully dealt with complex crystal such as $NdNbO_4$, $ZnZrNb_2O_8$ and $Li_2MgTi_3O_8$ [20-25] using the generalized P-V-L theory reported by *Zhang et al* [16-19], and built an relationship between the complex chemical bond theory and the microwave dielectric properties. In order to further generalize the use of the complex chemical bond theory in more complex crystals, therefore we decided to prepare and analyze the $Zn_3Nb_2O_8$ crystal using the complex chemical bond theory. Moreover, we proposed a new method for calculating the theoretical dielectric constant.

According to the complex chemical bond theory and our previous work [22-23], the complex crystals $Zn_3Nb_2O_8$ could be decomposed into the sum of binary crystals as follows:

$$Zn_3Nb_2O_8 = Zn(1)Zn(2)_2 Nb_2O(1)_2 O(2)_2 O(3)_2 O(4)_2$$

$$Zn_3Nb_2O_8 = Zn(1)_{1/3}O(3)_{2/3} + Zn(1)_{2/3}O(4)_{4/3} + Zn(2)O(1)_{6/5} + Zn(2)O(2)_{3/2}$$
$$+ Nb_{2/3}O(1)_{4/5} + Nb_{1/3}O(2)_{1/2} + Nb_{2/3}O(3)_{4/3} + Nb_{1/3}O(4)_{2/3}$$

$$Zn_3Nb_2O_8 = Zn(1)_{1/3}O(3)_{2/3} + Zn(1)_{1/3}O(4)^1_{2/3} + Zn(1)_{1/3}O(4)^2_{2/3} + Zn(2)_{1/3}O(1)^1_{2/5} + Zn(2)_{1/3}O(1)^2_{2/5}$$
$$+ Zn(2)_{1/3}O(1)^3_{2/5} + Zn(2)_{1/3}O(2)^1_{1/2} + Zn(2)_{1/3}O(2)^1_{1/2} + Zn(2)_{1/3}O(2)^1_{1/2} + Nb_{1/3}O(1)^1_{2/5}$$
$$+ Nb_{1/3}O(1)^2_{2/5} + Nb_{1/3}O(2)_{1/2} + Nb_{1/3}O(3)^1_{2/3} + Nb_{1/3}O(3)^2_{2/3} + Nb_{1/3}O(4)_{2/3}$$

2.2.1 The theoretical dielectric constant of a complex crystal

Any inorganic crystal possesses a dielectric constant which reflects the polarization ability and determined by the constituent atoms. Therefore, it is necessary to calculate the theoretical dielectric

constant of a given inorganic crystal. Based on the complex chemical bond theory, the theoretical

dielectric constant of the Zn_3NbO_8 ceramic is firstly calculated by the following formula.

$$\varepsilon_{(Zn_3Nb_2O_8)} = \sum (m\varepsilon_{(A_mO_n)}) \tag{4}$$

where $\varepsilon_{(Zn3NbO8)}$ represents the theoretical dielectric constant of the Zn_3NbO_8 ceramics, and A_mO_n is the

Zn-O bond and Nb/Ta-O bond. For any A_mO_n type compounds of μ bond, the dielectric constant ε^μ can

be defined as follows [27-28]:

$$\varepsilon^\mu = 1 + 4\pi\chi^\mu \tag{5}$$

where χ^μ is the susceptibility of any bond μ which is expressed as:

$$\chi^\mu = \frac{\left(\hbar\Omega_p^\mu\right)^2}{4\pi(E_g^\mu)^2} \tag{6}$$

where Ω_p^μ is the plasma frequency and described as the following equation:

$$(\Omega_p^\mu)^2 = \frac{4\pi(N_e^\mu)^* e^2}{m} D^\mu A^\mu \tag{7}$$

where e and m are the electronic charge and mass, respectively. $(N_e^\mu)^*$ is the number of valence

electronics of bond μ per cubic centimeter, which could be calculated from Ref.22. The correction

factors of order unity D^μ and A^μ are calculated as below:

$$D^\mu = \varDelta_A\varDelta_B - (\delta_A\delta_B - 1)[(Z_A^\mu)^* - (Z_B^\mu)^*]^2 \tag{8}$$

$$A^\mu = 1 - \frac{E_g^\mu}{4E_F^\mu} + \frac{1}{3}(\frac{E_g^\mu}{4E_F^\mu})^2 \tag{9}$$

The parameters $\varDelta$ and σ for D core corrections (Eq.6) are given in Table.1. The Z_A and Z_B are the

number of valence electrons on the A and B atoms of the μ bond, respectively. The E_g is the average

energy gap which could be obtained from Ref. 22, and the E_F is the Fermi energy which is given in

terms of the Fermi wave vector by

$$E_F^\mu = \frac{(\hbar k_F^\mu)^2}{2m} \tag{10}$$

$$k_F^\mu = [3\pi^2 (N_e^\mu)^*]^{1/3} \tag{11}$$

2.2.2 The lattice energy of a complex crystal

Generally, lattice energy is a dominant term in the thermodynamic analysis of the existence and stability of ionic solids [29-32]. According to the generalized P-V-L theory, the lattice energy for the single-bond crystal was consisted of the ionic and covalent parts. The ionic part mainly results from electrostatic interactions and repulsive interactions of the ion pairs, and another arises from the overlap of electron clouds. The calculation equation for the lattice energy U_{cal} of a complex crystal is written as [20-24]:

$$U_{cal} = \sum_\mu U_b^\mu \tag{12}$$

$$U_b^\mu = U_{bc}^\mu + U_{bi}^\mu \tag{13}$$

$$U_{bc}^\mu = 2100m \frac{(Z_+^\mu)^{1.64}}{(d^\mu)^{0.75}} f_C^\mu \tag{14}$$

$$U_{bi}^\mu = 1270 \frac{(m+n)Z_+^\mu Z_-^\mu}{d^\mu}(1 - \frac{0.4}{d^\mu})f_i^\mu \tag{15}$$

where U_{bc}^μ is the covalent part and U_{bi}^μ is the ionic part of μ bond. Z_+^μ and Z_-^μ are the valence states of cation and anion which constituted to the bond μ. f_i and f_c are the bond ionicity and bond covalency defined in Ref.23.

2.2.3 The bond energy of a complex crystal

For any specified inorganic crystal, shorter bond length correlates with higher bond energy and higher bond energy indicated that the system would more stable. *R. T. Sanderson* [33-35] reported that the bond energy could be obtained by the chemical bond and the electronegativity. Based on the

7

Sanderson bond energy theory, we proposed a modified method for calculating the bond energy of any complex crystal [21, 23]. The generalized bond theory was described as follows:

$$E = \sum_{\mu} E_b^{\mu} \tag{16}$$

where E is the bond energy for a complex crystal, and E_b is bond energy for the type μ bond, which is composed of nonpolar covalence energy E_c^{μ} and complete ionicity energy E_i^{μ} parts as follows:

$$E_b^{\mu} = t_c E_c^{\mu} + t_i E_i^{\mu} \tag{17}$$

where t_c and t_i are the covalent and ionic blending coefficients, which are defined as follows:

$$t_c + t_i = 1 \tag{18}$$

$$t_i = \left| \frac{(S_A - S_B)/\Delta S_B}{2} \right| \tag{19}$$

where S_A and S_B are the electronegativities of A and B ions. ΔS_B is the change for complete of an electron and has the value of 3.

The energy of the ionic form E_i^{μ} is the unit charge product divided by the bond length d^{μ}, adjusted to kcal/ mol by the factor 33200 when the bond length is pm.

$$E_i^{\mu} = \frac{33200}{d^{\mu}} \tag{20}$$

The nonpolar covalence energy E_c^{μ} is defined as:

$$E_c^{\mu} = \frac{(r_{cA} + r_{cB})}{d^{\mu}} (E_{A-A} E_{B-B})^{1/2} \tag{21}$$

where r_{cA} and r_{cB} are the covalent radii, E_{A-A} and E_{B-B} were the homonuclear bond energy obtained from the handbook of bond energies [36]. In this paper, r_{cZn}=118 pm, r_{cNb}=147 pm, r_{cTa}=146 pm and r_{cO}=63pm; E_{Zn-Zn}=22.2 kJ mol^{-1}, E_{Nb-Nb}=513 kJ mol^{-1}, E_{Ta-Ta}=390 kJ mol^{-1} and E_{O-O}=498.36 kJ mol^{-1}.

3. Results and discussion

3.1 Rietveld refinement by XRD date

8

Fig.1 shows the XRD patterns of Ta-doped sintered compounds. All the reflections are well matched with the PDF file no. 50-1725, and no any secondary phases are observed, which indicates the solid solution based on monoclinic-structured $Zn_3Nb_2O_8$ with the space group C2/c (no. 15) is identified at x=0.02 to 0.10. The diffraction peaks of the monoclinic phases slightly shift to a higher angle with the Ta content increase to 0.06, which indicated the decrease in cell volume, and then decreased. To study the details of crystal structures with Ta substitution, the Rietveld refinements using the Full-prof software are chose to analyze the crystal structure of the $Zn_3(Nb_{1-x}Ta_x)_2O_8$ ceramics. In order to reduce the influence of noises, strongest diffraction peaks of all samples are bigger than 10, 000. All parameters of interest including scale factors for all phases, zero point, background, unit-cell parameters, half-width, asymmetry parameters, atomic positional coordinates, temperature factors are refined step-by-step for avoiding correlations. The profile fits for the Rietveld refinement of $Zn_3(Nb_{0.94}Ta_{0.06})_2O_8$ is shown in Fig.2. The refined values of lattice parameters of x=0.06 samples are calculated as a=19.0393 Å, b=5.9030 Å, c=5.1967 Å, β=89.875° and V=584.0505 Å^3, the Rietveld discrepancy factors R_p and R_{wp} are 8.87% and 11.00%, respectively. The details of refined cell parameters, bond lengths and coordinates numbers are given in Table.2-4. As Table 2 shows, in the monoclinic structure of $Zn_3Nb_2O_8$, there are two types of Zn-O bonds. In the Zn(1)-O bond, there contains three different bond length, but six different lengths exist in the Zn(2)-O, which indicates two different oxygen octahedral would perform in the $Zn_3Nb_2O_8$ system. For the Nb-O bond, with the increasing of Ta content, the average long and short Nb-O distances have an obvious change. Both the long and short bond length decreased first and then increased, which indicates the substitution of Ta effectively decreased the cell volume. The decreased tendency in the Nb-site was due to the bigger relative atomic of Ta atom (180.9 g/mol) than Nb atom (92.91 g/mol), and the forces on Nb atom and O

9

atom would be enhanced when the lattice position of Nb-site was occupied by Ta^{5+} ions. Therefore, with the increasing of Nb^{5+} ions contents, the Nb-site bond length would decrease and the cell parameters of $Zn_3(Nb_{1-x}Ta_x)_2O_8$ ceramics decrease. With a further increase the Ta^{5+} ions contents, the cell parameters have an increasing tendency when x>0.08, this abnormal phenomenon suggests that there might has phase transformation in $Zn_3(Nb_{1-x}Ta_x)_2O_8$ ceramics decrease. *Birdeanu et al* [36]. reported that the $Zn_3Ta_2O_8$ phase belonged to the symmetry group C2/c, and its lattice parameters was: *a*=9.53 Å, *b*=8.39 Å, *c*=8.90 Å, β=89.875° and *V*=584.0505 Å^3. According to Vegard's law, if phase transformation was formed, the lattice parameters of $Zn_3(Nb_{1-x}Ta_x)_2O_8$ would change in the direction of $Zn_3Ta_2O_8$ phase.

3.2 Crystal structure analysis

The starting refined model for $Zn_3Nb_2O_8$ was considered from the inorganic crystal structure database (ICSD# 66147). Fig.3 shows the schematic crystal structures of monoclinic structure for $Zn_3Nb_2O_8$ crystal using the software of Crystal Maker. In the monoclinic structure, there contains four $Zn_3Nb_2O_8$ molecules per primitive cell, both Zn^{2+} and Nb^{5+} ions are connected with six oxygen atoms forming ZnO_6 and NbO_6 octahedron. The ZnO_6 and NbO_6 octahedron are arranged in order which formed a close packing from Fig.3 (a). And every NbO_6 octahedron layered are located in between in $Zn(1)O_6$ and $Zn(2)O_6$ octahedron layered by edge sharing which formed a "O" type arrangement in Fig.3 (b). In the $Zn_3Nb_2O_8$ system, the Nb^{5+} ionic occupy 8f Wyckoff positions whereas the four distinguishable oxygen atoms occupy the same positions 8f named O1, O2, O2, and O4. In this paper, the NbO_6 octahedron was composed with six different lengths of Nb-O bond. Due to the special crystal structure, the Ta^{5+} ions substitution for the Nb^{5+} would make a big contribution to the distortion for the NbO_6 octahedron. In order to analyze the effects of Nb^{5+} ions substitution with the Ta^{5+} ions on the

Nb-site oxygen octahedral distortion, the schematic distortion in NbO$_6$ for Zn$_3$(Nb$_{1-x}$Ta$_x$)$_2$O$_8$

(0.02≤x≤0.10) compounds is given in Fig.4 (a). In this paper, one criterion is set up by measuring the

octahedral distortion for the [NbO6] octahedron as followed formulas:

$$\Delta = \frac{1}{6}\sum\left[\frac{(d_{Nb-O(i)} - \overline{d}_{Nb-O(i)})}{\overline{d}_{Nb-O(i)}}\right]^2 \tag{22}$$

where $d_{Nb-O(i)}$ and $\overline{d}_{Nb-O(i)}$ present the Nb-O bond distance and the average of Nb-O bond distance,

respectively. Fig. 4 (b) shows the variation of the Nb-site oxygen octahedral distortion (Δ) for

Zn$_3$(Nb$_{1-x}$Ta$_x$)$_2$O$_8$ ceramics as a function of x values. With the increasing of the x values, the Δ

increased first and then decreased, which was due to the abnormal change in the Nb –site bond length,

could obtain the maximum values of 2.0247 % at x=0.06, comparing with the other x values. It

indicates that there would possible have an abnormal change on the microwave dielectric properties

when x≥0.06. In the following work, we will further discuss the intrinsic factors for variation of the

microwave dielectric properties.

3.3. *Raman spectroscopy*

Raman spectroscopy was usually considered to be more powerful than XRD analysis of physical

properties of the oxygen octahedron and its arrangement [37-39]. Narrow and intense peaks are usually

observed for well-ordered structures. There have been many reports of Raman scattering on microwave

dielectric materials [40-45]. However, the Raman spectra have not been widely studied in Zn$_3$Nb$_2$O$_8$

system. For the monoclinic structure of the Zn$_3$Nb$_2$O$_8$ crystal (space group C2/c) with four structural

units per unit cell, the cation Zn1 and Zn2 occupy the 4e sites of C_2 symmetry, whereas both the Nb

and O ions occupy the 8f sites with C_1 symmetry. Based on the group theory reported by *Rousseau et al.*

[46], the irreducible representations all the active modes are given below:

$$\Gamma = 19A_g + 20B_g + 19A_u + 20B_u$$

where all the 'g' vibrations are Raman active mode, whereas 'u' vibrations are IR active mode. According to group theory analysis, there are 39 Raman active modes possible for the $Zn_3Nb_2O_8$ system. Table.5 shows the calculation results of expected 39 theoretical vibrational frequencies and vibrational intensity for Raman active mode using the Fist-principle theory by the software of Mat Studio. Fig.5 shows the indentified Raman spectra of $Zn_3(Nb_{1-x}Ta_x)_2O_8$ (x=0.02-0.10) in the range of 50-1000cm^{-1}. Based on the recent reported by *Graça et al*. [47], the vibrations with the smallest frequencies are associated with the $[NbO_4]^{-3}$ units, and the symmetric Nb-O vibration modes in the $[NbO_6]$ octahedron appears the strongest peaks and 200 to 300 cm^{-1}, and the anti-symmetric vibration modes can be given in between 400 and 500 cm^{-1} and 600 to 700 cm^{-1}. When the Ta^{5+} substitution for Nb^{5+}, the $[NbO_6]$ octahedron became distorted, which possibly affect the position and intensity of peaks of internal modes. There are great changes in the vibration modes related to stretching motions (v_{15} and v_{39}) which belong to Nb-O bond. As shown in Fig.5, with the increasing of x values, the intensity of v_{39} mode increase to a maximum at x=0.06 and then decreased. However the v_{15} would simply fade away with the increasing of the x values, when x=0.10, the v_{15} mode wouldn't be appeared in the Raman spectra. In suggests that the substitution Ta^{5+} ions for Nb^{5+} ions actually affect the vibration modes of Nb-O bond in the $Zn_3Nb_2O_8$ system, and there have phase transformation in the $Zn_3(Nb_{1-x}Ta_x)_2O_8$ (x=0.02-0.10) ceramics when x=0.08.

3.4. Microstructure and bulk densities analysis

The SEM images of $Zn_3(Nb_{1-x}Ta_x)_2O_8$ (x=0.02-0.10) ceramics sintered at 1175 °C are provided in Fig. 6. With the x values increase from 0.02 to 0.06, the grain size have an increasing tendency, homogeneous grains and smooth surface would be appeared in x=0.06. With a further increasing of Ta

ions contents, the grains have no obvious change, and all the specimens have well-packed grains and estimated mean particle size was in the range of 10-13 μm, which show well-densified SEM photos.

Fig.7 shows the theoretical density and relative density for $Zn_3(Nb_{1-x}Ta_x)_2O_8$ ceramics with different x values. Notice that the theoretical densities exhibit an increasing tendency with the x values increased, which is because that higher Ta substitution contents would result in a smaller cell volume. Therefore, the theoretical densities would keep and increasing tendency based on Eq.(2). However, the relative densities presents no directly relationship with the x value, and all the relative densities are in the range of 96.65%~96.75%. The high densification of specimens is due to the low porosity and well-grain growth, which would be demonstrated from Fig.6.

3.6. Microwave dielectric properties analysis

At microwave frequency band, the dielectric constant is mainly influenced by the dielectric polarizability, as well as the relative density and second phase [48-50]. In our experiments, the relative density and second phase are not under consideration in the ε_r values due to pure phase from XRD and high-densified specimens from the SEM photos. Therefore, in order to evaluate the intrinsic factors of the ε_r values, we have calculated the theoretical dielectric constant ε_{cal}. The details ε_{cal} of the $Zn_3(Nb_{1-x}Ta_x)_2O_8$ (x=0.02-0.10) ceramics are given in Table.6. As Table.6 shows, the Nb-O bond makes more contribution to the ε_{cal} than the Zn-O bond, which confirmed that the Nb-site oxygen octahedral have vital effect on the microwave dielectric properties. Fig.8 (a) presents the experimental dielectric constants ε_r of $Zn_3(Nb_{1-x}Ta_x)_2O_8$ ceramics with x=0.02-0.10 as a function of calculated dielectric constants ε_{cal}. Observed that the ε_r keep a similar variation tendency with the ε_{cal}. With the x increase from x=0.02 to x=0.08, both ε_r and ε_{cal} could reach a maximum of 22.61 and 22.03. In the view of above finding, it suggests that the ε_r could be calculated using the complex chemical bond theory in the

13

further research.

For the microwave dielectric materials, the Q×f values are usually controlled by the following two main fields, the intrinsic losses and extrinsic losses. The intrinsic losses are mainly caused by lattice vibration modes, while the others are dominated by such as second phases, oxygen vacancies, grain boundaries, and densification or porosity [51-53]. In this work, the effect of extrinsic losses are minimal due to the densified compounds. Our recent works indicates that the Q×f values of ABO_4 compounds with oxygen octahedron structure are observed to relate to the B-site lattice energy [20-24]. With an increase in the lattice energy, the Q×f values would increase. Based on the complex chemical bond theory, the calculated results of the lattice energy are shown in Table.7. The obtained results reveal that the Nb-site lattice energy U_{Nb-O} have more contribution to the lattice energy in $Zn_3Nb_2O_8$, which indicates that the variation of Q×f values in $Zn_3(Nb_{1-x}Ta_x)_2O_8$ is affect by the U_{Nb-O}. With the increasing of the x values, the Nb-site lattice energy increased and reached its maximum at x=0.06. According to analyze of octahedral distortion shown in Fig.4 (b), the variation of Nb-site lattice energy exhibits an similar tendency with the Nb-site octahedral distortion, which is because that Nb-site octahedral distortion play a key role in crystal structure. Therefore, the change in the crystal structure, like bond length, could effectively affect the lattice energy. Fig.8 (b) shows the Q×f values of $Zn_3(Nb_{1-x}Ta_x)_2O_8$ ceramics with x=0.02-0.10 as a function of U_{Nb-O}. We can discover that with the Ta contents increasing, the U_{Nb-O} have the same change with the Q×f values. When x =0.08, the lattice energy decreased, the Q×f values decreased.

In the microwave dielectric materials system, the temperature coefficient of resonant frequency τ_f value reveal the stability of the system, and smaller $|\tau_f|$ value indicates the system would more stable. As we all known, the stability of one system would be characterized by the bond energy, and higher

14

bond energy correlates more stable system. That is to say, the variation of $|\tau_f|$ value could be predicted

by the bond energy. Table.8 presents the calculated Nb-site bond energy with different Ta substitution

contents. The τ_f values of $Zn_3(Nb_{1-x}Ta_x)_2O_8$ ceramics with x=0.02-0.10 as a function of Nb-site bond

energy are given in Fig. 8(c). As shown in Fig.8 (c), the change of $|\tau_f|$ value was in accordance with the

Nb-site bond energy. More stable materials of $Zn_3(Nb_{1-x}Ta_x)_2O_8$ with maximum of Nb-site bond energy

3612.11 KJ/mol would appear at x=0.08.

4. Conclusions

Microwave dielectric properties of $Zn_3(Nb_{1-x}Ta_x)_2O_8$ (0.02≤x≤0.10) ceramics were investigated via

solid state reaction method. The structural parameters were calculated by Rietveld refinement method

based on XRD data, and the vibrational phonon modes were analyzed systematically for the first time.

In the monoclinic structure of $Zn_3Nb_2O_8$, with the increasing of Ta substitution contents, the Nb-site

oxygen octahedral distortion would have an obvious change. Later, new method for calculation the

theoretical dielectric constant is proposed. For the $Zn_3(Nb_{1-x}Ta_x)_2O_8$ ceramics, the dielectric constant

could be predicted by the theoretical calculation. The increased tendency of Q×f values were due to the

higher lattice energy of the specimens. The τ_f of the specimens was mainly depended on the Nb-site

bond energy, with an increase in the bond energy, the $|\tau_f|$ value would decrease which indicates the

system become stable. In summary, the $Zn_3(Nb_{0.94}Ta_{0.06})_2O_8$ ceramics possesses excellent microwave

dielectric properties with an ε_r value of 20.95, Q ×f value of 111,800 GHz and τ_f value of -62.56

ppm/°C sintered at 1175 °C.

Acknowledgments

Hai-Tao Wu for his help in XRD, Raman experimental.

References

[1] M. T. Sebastian, Dielectric materials for wireless communication, Elsevier publishing group, 2008.

[2] S. D. Ramarao and V. R. K. Murthy, *Dalton. Trans*., 2015, 44, 2311-2324.

[3] I. M. Reaney, D. Iddles, *J. Am. Ceram. Soc*., 2006, 89, 2063-2072.

[4] M. T. Sebastian, H. Jantunen, *Int. Mater. Rev*., 2008, 53, 57-90.

[5] J. Guo, C. A. Randall, G. Q. Zhang, D. Zhou, Y. Y. Chen, *J. Mater. Chem. C*., 2014, 2, 7364-7372.

[6] C. Nico, M. R. N. Soares, J. Rodrigues, M. Matos, et al. *J. Phys. Chem. C*., 2011, 115, 4879-4886.

[7] M. R. N. Soares, S. Leite, C. Nico, M. Peres, et al. *J. Eur. Ceram. Soc*., 2011, 31, 501-506.

[8] D. W. Kim, J. H. Kim, J. R. Kim, K. S. Hong, *Jpn. J. Appl. Phys*., 2001, 40, 5994-5998.

[9] P. S. Anjana, I. N. Jawahar, M. T. Sebastian, *J. Mater. Sci.: Mater. Electron*., 2009, 20, 587-596.

[10] Y. C. Lee, C. H. Lin, I. N. Lin, *Mater. Chem. Phys*., 2003, 79, 124-128.

[11] M. C. Wu, K. T. Huang, W. F. Su, *Mater. Chem. Phys*., 2006, 98, 406-409.

[12] Y. C. Liou, H. M. Cheng, W. C. Tsai, *Ceram. Int*., 2009, 35, 2135-2138.

[13] W. R. Yang, P. C. Yu, C. L. Huang, *J. Alloy. Compd*., 2013, 581, 257-262.

[14] C. L. Huang, W. R. Yang, P. C. Yu, *J. Eur. Ceram. Soc*., 2014, 34, 277-284.

[15] L. X. Li, H. Sun, X. S. Lv, S. Li, *J. Mater. Sci.: Mater. Electron*., 2015, 26, 7026-7031.

[16] Z. J. Wu, Q. B. Meng, S. Y. Zhang, *Phys. Rev. B*., 1998, 58, 958-962.

[17] Q. B. Meng, Z. J. Wu, S. Y. Zhang, *J. Phys. Cond. Mat*., 1998, 10, 85-88.

[18] D. T. Liu, S. Y. Zhang, Z. J. Wu, *Inorg. Chem*., 2003, 42, 2465-2469.

[19] Z. J. Wu, S. Y. Zhang, *Int. J. Quantum. Chem*., 1999, 73, 433-437.

[20] P. Zhang, Y. G. Zhao and L. X. Li, *Phys. Chem. Chem. Phys*., 2015, 17, 16692-16698.

[21] P. Zhang, Y. G. Zhao, *J. Alloy. Compd.*, 2015, 654, 240-245.

[22] P. Zhang, Y. G. Zhao and X. Y. Wang, *Dalton. Trans.*, 2015, 44, 10932-10938.

[23] P. Zhang, Y. G. Zhao and X. Y. Wang, *Dalton. Trans.*, 2015, 44, 16684-16693.

[24] P. Zhang, Y. G. Zhao, *J. Alloy. Compd.*, 2015, 647, 386-391.

[25] Y. G. Zhao, P. Zhang, *RSC Adv.,* 2015, 5, 97746-97754.

[26] K. P. F. Siqueira, R. L. Moreira, *Chem. Mater.*, 2010, 22, 2668-2674.

[27] B. F. Levine, *J. Chem. Phys.*, 1973, 59, 1463-1486.

[28] B. F. Levine, *Phys. Rev. B.*, 1973, 7, 2600-2626.

[29] J. C. Phillips, *Phys. Rev. Lett.*, 1969, 22, 705-708.

[30] J. C. Phillips,   *Phys. Rev. Lett.*, 1967, 20, 550-553.

[31] A. F. Kapustinskii, *Rev. Chem. Soc.*, 1956, 10, 283-294.

[32] L. Glasser, H. D. B. Jenkins, *J. Am. Chem. Soc.*, 2000, 122, 632-638.

[33] R. T. Sandderson, *Inorg. Nucl. Chem.*, 1966, 28, 1553-1565.

[34] R. T. Sandderson, *Inorg. Nucl. Chem.*, 1968, 30, 375-393.

[35] R. T. Sandderson, *J. Am. Chem. Soc.*, 1983, 105, 2259-2261.

[36] R. T. Sandderson, Chemical bonds and bond energy, Academic Press: New York,1971.

[37] M. Birdeanu, I. Sebarchievici, A. V. Birdeanu, B. Taranu, F. Peter, and E. Fagadar-Cosma. *Dig. J.*

N8nomater. Bios. 2015, 10, 543-555.

[38] J. M. Jehng, I. E. Wachs, *Chem. Mater.*, 1991, 3, 100-107.

[39] D. Zhou, L. X. Pang, J. Guo, et al. *Inorg. Chem.*, 2014, 53, 1048-1055.

[40] S. K. Singh, V. R. K. Murthy, *Mater. Chem. Phys.*, 2015, 160, 187-193.

[41] M. L. Sanjuan and M. A. Laguna, *Phys. Rev. B*, 2001, 64, 174305.

[42] C. T. Chia, Y. C. Chen, H. F. Cheng, I. N. Lin, *J. Appl. Phys.*, 2003, 94, 3365-3370.

[43] H. Zheng, I. M. Reaney, R. Ubic, et al. *J. Mater. Res.*, 2004, 19, 488-495.

[44] D. Zhou, W. B. Li, L. X. Pang, et al. *Dalton. Trans.*, 2014, 43, 7290-7297.

[45] J. Guo, D. Zhou, Y. Li, et al. *Dalton. Trans.*, 2014, 43, 11888-11896.

[46] D. L. Rousseau, R. P. Bauman, *J. Raman. Spectrosc.*, 1981, 10, 253-290.

[47] M. P. F. Graça, M. V. Peixoto, N. Ferreira, J. Rodrigues, *J. Mater. Chem. C.*, 2013, 1, 2913-2919.

[48] D. Zhou, L. X. Pang, J. Guo, et al. *J. Mater. Chem.*, 2012, 22, 21412-21419.

[49] P. Zhang, Z. K. Song, Y. Wang, Y. M. Han, H. L. Dong, L. X. Li, *J. Alloy. Compd.*, 2013, 581, 741-746.

[50] P. Zhang, Z. K. Song, Y. Wang, L. X. Li, *J. Am. Ceram. Soc.*, 2014, 97, 976-981.

[51] C. L. Huang, J. Y. Chen, *J. Am. Ceram. Soc.*, 2010, 93, 1248-1251.

[52] D. Zhou, L. X. Pang, J. Guo, et al. *Inorg. Chem.* 2011, 50, 12733-12738.

[53] D. Zhou, L. X. Pang, Z. M. Qi. *Inorg. Chem.* 2014, 53, 9222-9227.

Figure captions

Fig.1 XRD patterns of $Zn_3(Nb_{1-x}Ta_x)_2O_8$ ceramics with different x values sintered at 1175 ^{o}C for 4h.

Fig.2 The structural refinement patterns of the $Zn_3(Nb_{0.94}Ta_{0.06})_2O_8$ ceramic.

Fig.3 Schematic crystal structure of $Zn_3Nb_2O_8$, (a): view at b-axis direction; (b) view at c-axis direction.

Fig.4 (a) Schematic distortion in NbO_6 for $Zn_3(Nb_{1-x}Ta_x)_2O_8$ (0.02≤x≤0.10) compounds; (b) the Nb-site

octahedral distortion for $Zn_3(Nb_{1-x}Ta_x)_2O_8$ as a function of x values.

Fig.5 The Raman spectra of for $Zn_3(Nb_{1-x}Ta_x)_2O_8$ with different x values sintered at 1175 ^{o}C for 4h.

Fig.6. SEM images of the samples with x=0.02 to 0.10 sintered at 1175 ^{o}C for 4h.

Fig.7. The theoretical density and relative density of $Zn_3(Nb_{1-x}Ta_x)_2O_8$ (0.02≤x≤0.10) ceramics.

Fig.8 (a) The experimental dielectric constants ε_r of $Zn_3(Nb_{1-x}Ta_x)_2O_8$ ceramics with x=0.02-0.10 as a

function of calculated dielectric constants ε_{cal}; (b) The Q×f values of $Zn_3(Nb_{1-x}Ta_x)_2O_8$ ceramics with

x=0.02-0.10 as a function of Nb-site lattice energy; (c) The τ_f values of $Zn_3(Nb_{1-x}Ta_x)_2O_8$ ceramics with

x=0.02-0.10 as a function of Nb-site bond energy.

Fig. 1

Dalton Transactions Accepted Manuscript
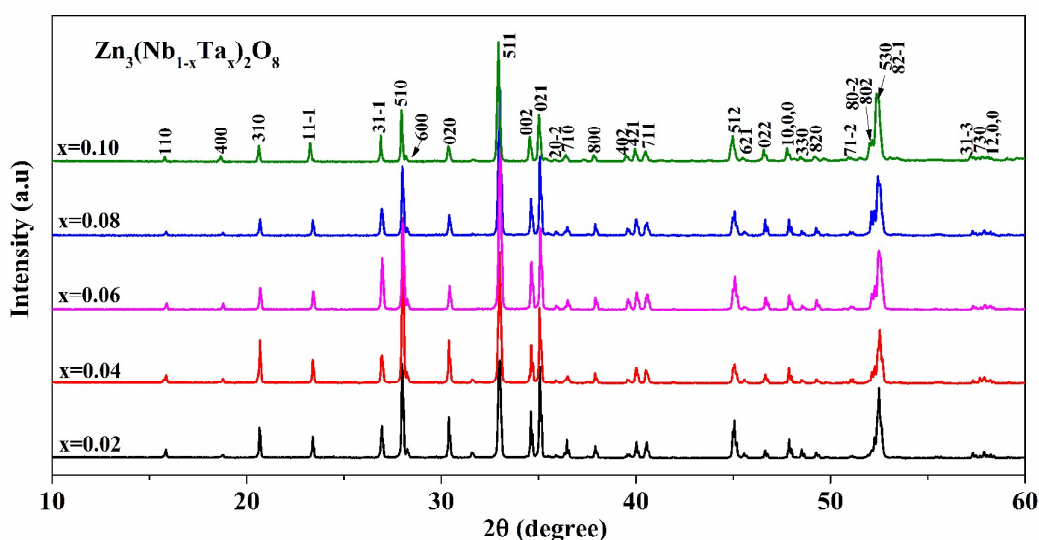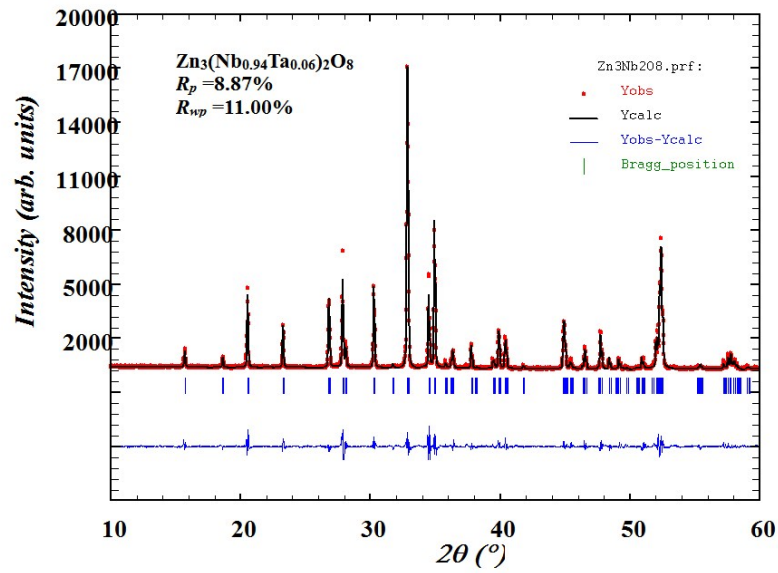
Fig.2
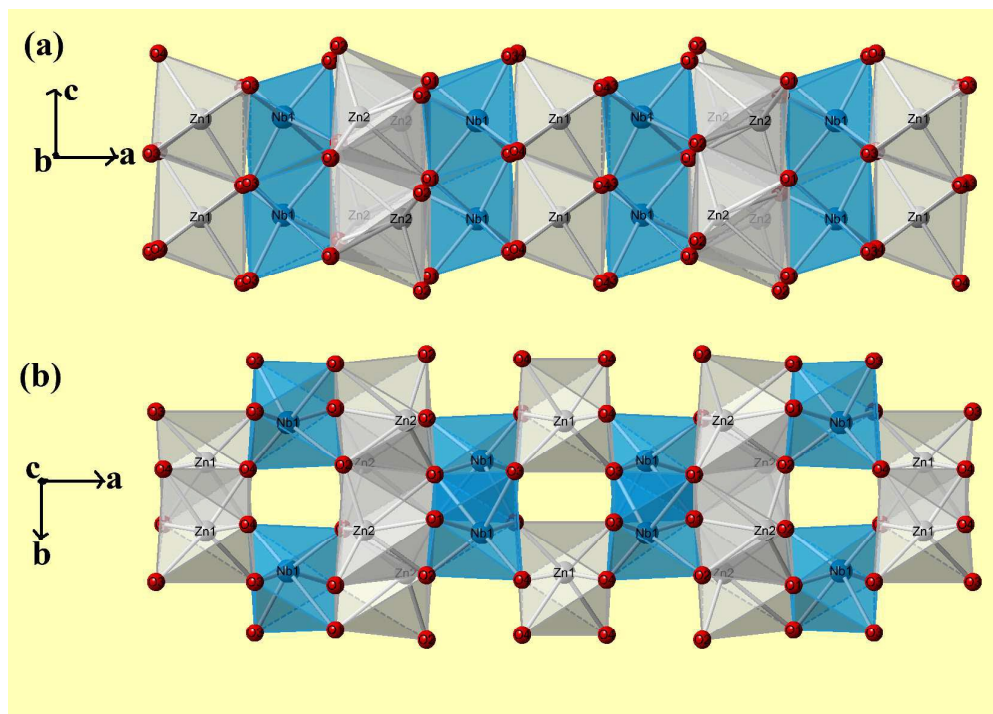
Fig.3
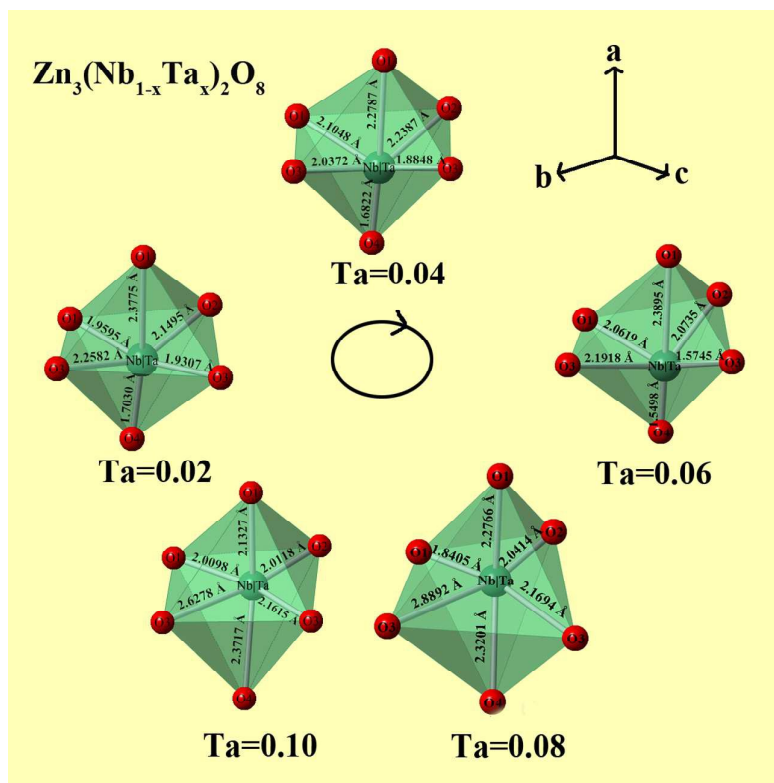
Fig.4 (a)
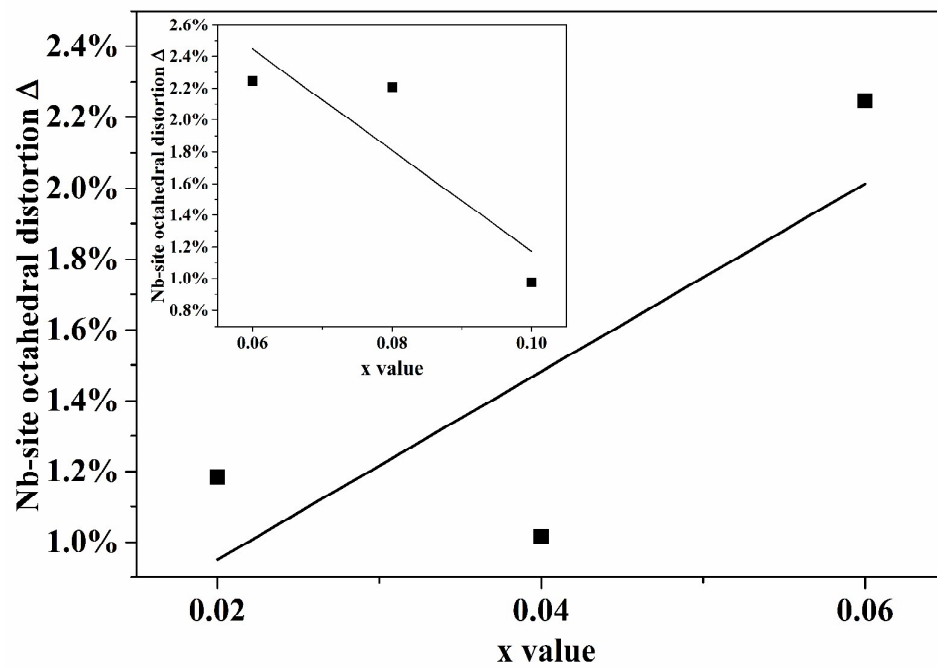
Fig.4 (b)
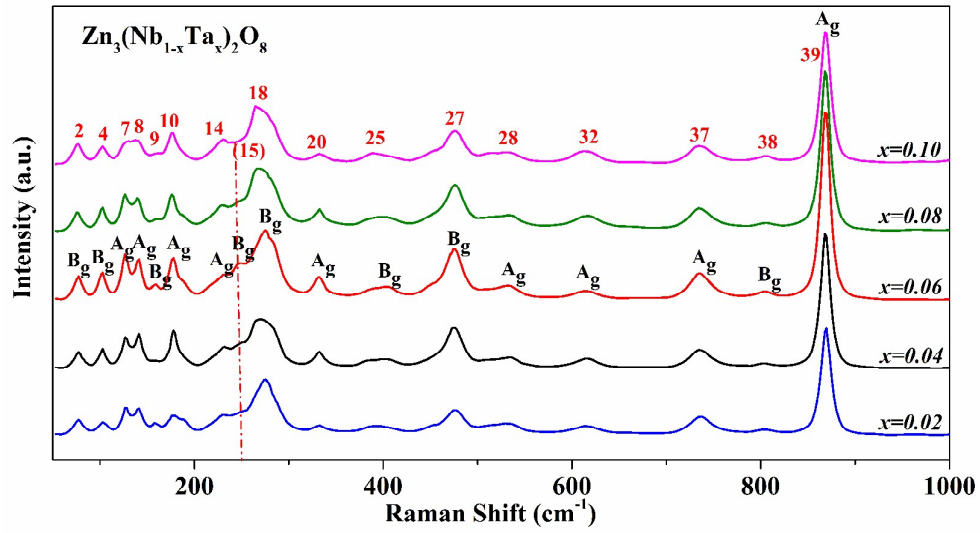
Fig. 5
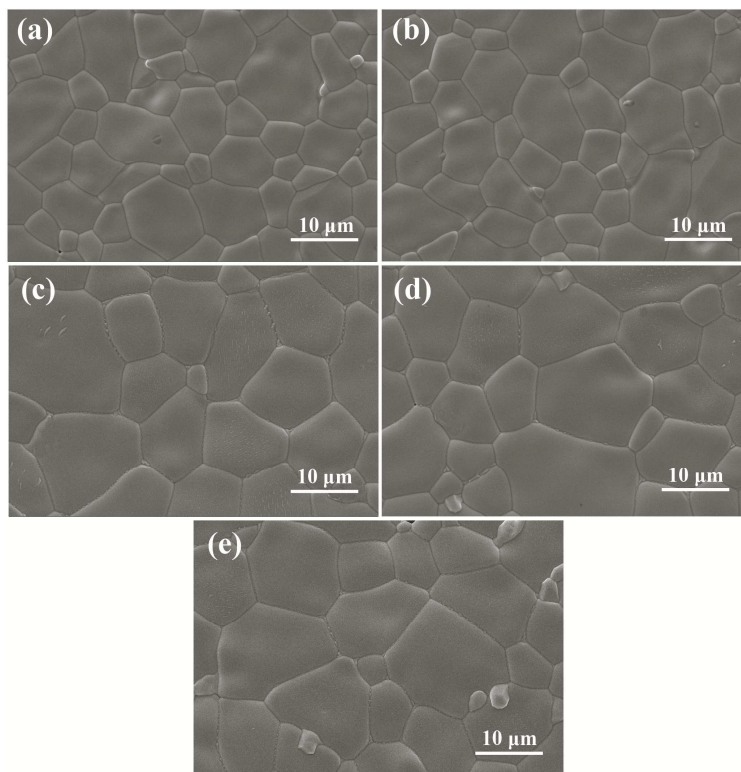
Fig. 6
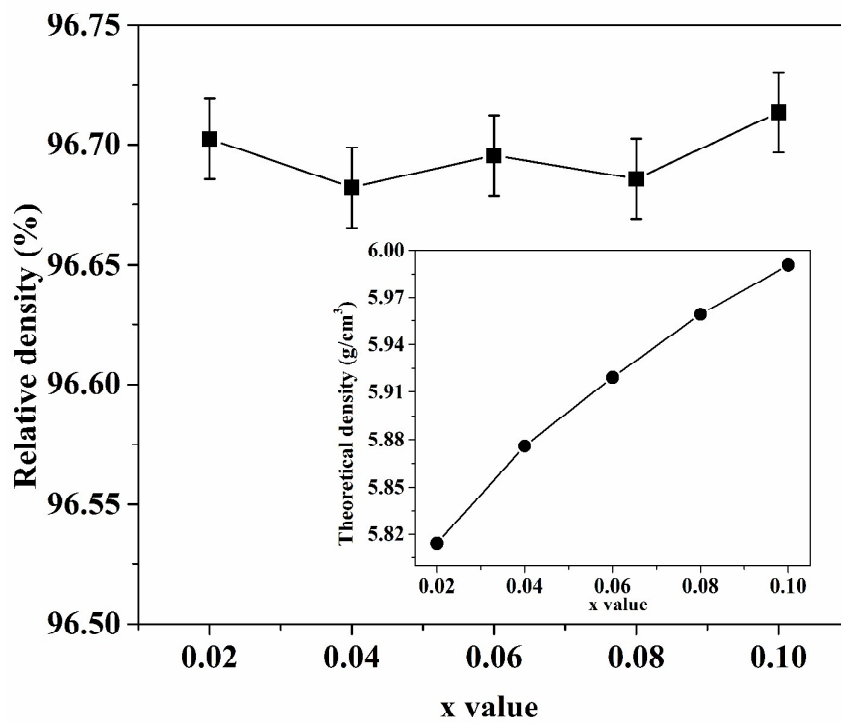
Fig. 7
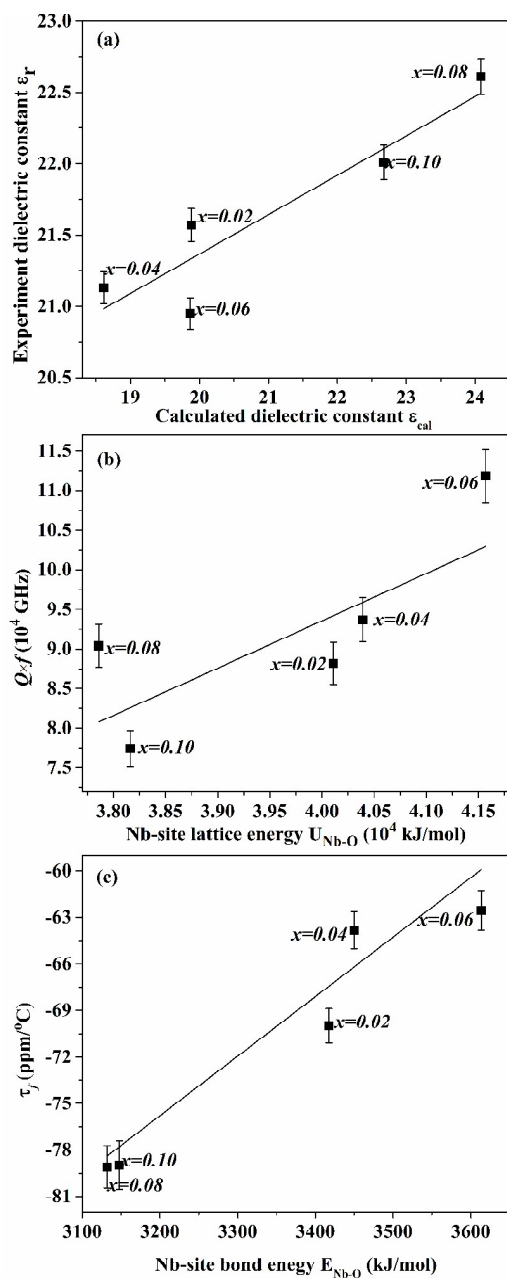
Fig. 8

Table.1 Parameters for D core corrections for atoms in period 1-6.

Period	Δ	σ
1	1.0	1.0
2	1.0	1.0
3	1.0	1.0
4	1.12	1.0025
5	1.21	1.0050
6	1.31	1.0075

Table.2 Refined lattice parameters (*a, b, c, V* and *β*) and Rietveld discrepancy (*R_p* and *R_{wp}*) for

$Zn_3(Nb_{1-x}Ta_x)_2O_8$ (0.02≤x≤0.10) ceramics.

x value	*a (Å)*	*b(Å)*	*c(Å)*	*β(°)*	*V(Å³)*	*R_p(%)*	*R_{wp}(%)*
x=0.02	19.0671	5.9073	5.2077	89.830	586.5674	7.52	11.1
x=0.04	19.0415	5.9019	5.2000	89.855	584.3723	7.03	9.28
x=0.06	19.0393	5.9030	5.1967	89.875	584.0505	8.87	11.00
x=0.08	19.0345	5.9027	5.1985	89.870	584.0757	10.40	11.20
x=0.10	19.0450	5.9047	5.2012	89.843	584.8988	7.34	9.69

Table.3 Bond length (Å) for $Zn_3(Nb_{1-x}Ta_x)_2O_8$ (0.02≤x≤0.10) ceramics.

Type	*Ta=0.02*	*Ta=0.04*	*Ta=0.06*	*Ta=0.08*	*Ta=0.10*
Zn(1)-O(3)×2	1.9320	2.2350	2.3964	1.5510	1.7880
Zn(1)-O(4)^1×2	2.0843	2.1481	2.3309	1.8273	1.6715
Zn(1)-O(4)^2×2	2.3950	2.4005	2.5157	2.1930	1.9955
Zn(2)-O(1)^1×1	1.8344	1.9561	1.8089	1.9026	1.9465

Zn(2)-O(1)²×1	2.4634	2.3873	2.5743	2.4716	2.7067
Zn(2)-O(1)³×1	2.7637	2.4574	2.2703	2.8471	2.7122
Zn(2)-O(2)¹×1	1.8591	1.7692	1.7494	1.9283	1.7523
Zn(2)-O(2)²×1	1.8807	1.8652	1.7915	1.9381	2.0255
Zn(2)-O(2)³×1	2.2740	2.1438	2.3674	2.1553	2.3575
Nb/Ta-O(1)¹ ×1	1.9595	2.1048	2.0619	1.8405	2.0098
Nb/Ta-O(1)² ×1	2.3775	2.2787	2.3895	2.2766	2.1327
Nb/Ta-O(2) ×1	2.1495	2.2387	2.0735	2.0414	2.0118
Nb/Ta-O(3)¹ ×1	1.9307	1.8848	1.5745	2.1694	2.1615
Nb/Ta-O(3)²×1	2.2582	2.0372	2.1918	2.8892	2.6278
Nb/Ta-O(4) ×1	1.7030	1.6822	1.5498	2.3201	2.3717

Table.4 Refined atomic fractional coordinates from XRD data for $Zn_3(Nb_{0.94}Ta_{0.06})_2O_8$ ceramic.

Element	*Wyckoff site*	*x*	*y*	*z*	*OCC*
Zn1	4e	0.00000	0.65850	0.25000	0.50
Zn2	8f	0.27920	0.17130	0.24900	1.00
Nb	8f	0.11835	0.16174	0.25493	0.94
Ta	8f	0.11835	0.16174	0.25493	0.06
O1	8f	0.30800	0.39500	0.46200	1.00
O2	8f	0.20830	0.29800	0.09100	1.00
O3	8f	0.40610	0.35000	0.0400	1.00
O4	8f	0.07970	0.34900	0.40900	1.00

Table.5 The calculated phonon modes parameters (Wavenumbers $w(cal)$ (cm^{-1}) and Intensity $I(cal)$) and experiment phonon modes parameters at x=0.06 (Wavenumbers $w(0.06)$ (cm^{-1})) from Raman analysis for $Zn_3(Nb_{1-x}Ta_x)_2O_8$ (0.02≤x≤0.10) ceramics.

Band	Symmetry	w(cal)	I(cal)					Bond(0.06)	w(0.06)
1	A_g	47.02	49.26	20	A_g	331.19	98.72	2	77.15
2	B_g	79.23	49.80	21	B_g	339.07	16.59	4	102.85
3	A_g	90.18	75.80	22	A_g	341.60	368.64	7	126.64
4	B_g	102.47	28.52	23	B_g	355.38	40.27	8	142.25
5	B_g	109.06	13.04	24	A_g	365.67	124.77	9	159.48
6	B_g	121.86	6.31	25	B_g	427.12	107.79	10	177.68
7	A_g	123.58	28.35	26	A_g	452.56	385.74	14	232.04
8	A_g	139.19	95.08	27	B_g	488.45	192.94	15	250.09
9	B_g	145.32	50.83	28	A_g	544.30	105.03	18	275.29
10	A_g	167.39	377.02	29	B_g	548.02	15.84	20	332.64
11	B_g	192.18	4.96	30	B_g	566.34	101.72	25	403.80
12	A_g	195.65	6.63	31	A_g	574.64	363.32	27	474.44
13	B_g	203.15	57.63	32	A_g	582.15	1651.91	28	544.96
14	A_g	231.06	99.07	33	B_g	642.99	15.37	32	613.91
15	B_g	257.43	49.78	34	B_g	671.46	415.91	37	734.17
16	A_g	262.57	109.09	35	A_g	690.54	325.09	38	804.45
17	A_g	271.73	137.78	36	B_g	749.17	13.47	39	867.92
18	B_g	277.36	135.24	37	A_g	780.63	1137.48		
19	B_g	295.95	24.29	38	B_g	871.21	213.14		
20	A_g	331.19	98.72	39	A_g	920.03	5285.74		

Table.6 The calculated dielectric constant (ε_{cal}) using complex chemical bond theory for $Zn_3(Nb_{1-x}Ta_x)_2O_8$ (0.02≤x≤0.10) ceramics.

Bond Type	ε_{cal}				
	Ta=0.02	Ta=0.04	Ta=0.06	Ta=0.08	Ta=0.10

Zn(1)-O(3)×2	4.5726	5.2446	6.1048	3.8609	4.4451
Zn(1)-O(4)[1]×2	5.0389	4.9745	5.8666	4.6921	4.1016
Zn(1)-O(4)[2]×2	6.1045	5.7914	6.5584	5.9816	5.1075
Zn(2)-O(1)[1]×1	2.2377	2.2544	2.2130	2.5052	2.4916
Zn(2)-O(1)[2]×1	2.9362	2.6972	3.0843	3.2682	3.5451
Zn(2)-O(1)[3]×1	3.3660	2.7797	2.6931	3.9223	3.5545
Zn(2)-O(2)[1]×1	2.9868	2.7253	2.8198	3.4014	3.0074
Zn(2)-O(2)[2]×1	3.0205	2.8595	2.8820	3.4199	3.4879
Zn(2)-O(2)[3]×1	3.7052	3.2890	3.8868	3.8544	4.1744
Nb/Ta-O(1)[1] ×1	2.1317	2.1799	2.2366	2.1933	2.3268
Nb/Ta-O(1)[2] ×1	2.6223	2.3683	2.6367	2.7574	2.4787
Nb/Ta-O(2) ×1	3.6076	3.5906	3.4391	3.7727	3.5827
Nb/Ta-O(3)[1] ×1	5.5587	5.0611	4.2708	7.500	7.1890
Nb/Ta-O(3)[2]×1	7.0579	5.6452	6.7199	12.7263	10.1299
Nb/Ta-O(4) ×1	4.7006	4.3749	4.1933	8.3974	8.4018
ε_{cal}	19.8823	18.6119	19.8684	24.0844	22.6745

Table.7 Lattice energy for $Zn_3(Nb_{1-x}Ta_x)_2O_8$ (0.02≤x≤0.10) ceramics.

	Lattice energy U (kJ/mol)				
Bond Type	*Ta=0.02*	*Ta=0.04*	*Ta=0.06*	*Ta=0.08*	*Ta=0.10*
Zn(1)-O(3)×2	1165	1037	982	1387	1242
Zn(1)-O(4)[1]×2	1098	1070	1004	1222	1309
Zn(1)-O(4)[2]×2	982	979	944	1058	1139

Zn(2)-O(1)^1×1	1334	1272	1348	1300	1278
Zn(2)-O(1)^2×1	1064	1090	1027	1062	986
Zn(2)-O(1)^3×1	969	1066	1135	946	985
Zn(2)-O(2)^1×1	1240	1286	1298	1208	1297
Zn(2)-O(2)^2×1	1229	1235	1275	1203	1162
Zn(2)-O(2)^3×1	1061	1110	1028	1108	1032
Nb/Ta-O(1)^1 ×1	7748	7348	7460	8102	7598
Nb/Ta-O(1)^2 ×1	6680	6912	6653	6904	7265
Nb/Ta-O(2) ×1	6558	6359	6740	6811	6888
Nb/Ta-O(3)^1 ×1	6413	6529	7403	5868	5887
Nb/Ta-O(3)^2×1	5695	6164	5828	4669	5046
Nb/Ta-O(4) ×1	7016	7079	7482	5571	5477
$U_{Nb\text{-}O}$	40110	40391	41566	37925	38161

Table.8 Calculated Nb-site bond energy of $Zn_3(Nb_{1-x}Ta_x)_2O_8$ (0.02≤x≤0.10) ceramics.

Bond Type	Bond Energy E (kJ/mol)				
	Ta=0.02	*Ta=0.04*	*Ta=0.06*	*Ta=0.08*	*Ta=0.10*
Nb/Ta-O(1)^1	592.38	550.66	561.27	627.83	574.07
Nb/Ta-O(1)^2	488.23	508.64	487.32	507.57	540.99
Nb/Ta-O(2)	540.02	517.72	558.13	566.05	573.50
Nb/Ta-O(3)^1	601.22	614.93	735.01	532.65	544.78
Nb/Ta-O(3)^2	514.03	568.93	528.00	399.95	439.06
Nb/Ta-O(4)	681.61	689.00	740.73	498.05	486.47

E_{Nb-O}	3417.49	3449.88	3613.46	3132.10	3147.87

$Zn_3(Nb_{1-x}Ta_x)_2O_8$